

Advanced Grid Connectivity Using Hybrid Solar, Wind, and Battery Technologies

Mukundswamy M S¹, Abhishek V², Abhinav Yadav³, Rahil M⁴, Yogeshwar C⁵, Dr G V Jayaramaiah⁶

^{1,2,3,4,5,6}Department of Electrical and Electronics Engineering, Dr. Ambedkar Institute of Technology, Bangalore, Karnataka, India.

Emails: mukundswamym@gmail.com¹, abhishekgowdaabhi16@gmail.com², abhinav2002yadav@gmail.com³, rm725366@gmail.com⁴, yashuchassan@gmail.com⁵, gvjayaram.ee@drait.edu.in⁶

Abstract

Global warming has led to the proliferation of electric vehicles, which seem to be the best option for internal combustion engines. With so many electric cars on the road, it's not practical or economical to charge cars using traditional power lines. Using renewable energy when charging stations control the electric vehicle. The project describes the charging system (SWCM) based on solar energy (250W), 15 modules in series and 2 parallel in series, and wind power (5.78kW) to generate electricity to charge the battery of the EV (electric vehicle). The regenerative charging station consists of wind turbines and PV (solar photovoltaic) modules. Charging mechanisms based on wind energy reduce CO₂ and CO₂-related emissions by reducing the need for fossil fuels to generate electricity. EV (electric vehicle) charging stations containing solar, wind, grid and BESS (battery energy storage systems) are designed according to the current situation. Additional grid support is also assumed to provide uninterrupted power to the charging stations without placing additional load on the grid. To balance the requirements, the system is connected to the grid via a three-phase bidirectional DC-AC (alternating current) frequency converter. The results show that the regenerative power generator is suitable for charging electric vehicles and creating a Pollution-free environment. The results are demonstrated with a MATLAB simulation run.

Keywords: Bi-directional, Vehicle to home, Vehicle to grid, Converters.

1. Introduction

New hybrid vehicle charging stations are equipped with various energy sources such as photovoltaic systems, wind energy systems, AC, battery packs as the main energy storage system and grid-connected inverters for always-on energy. This article describes progress on a solar-wind hybrid charging station that uses power converters and bi-directional DC-DC converters to balance DC voltages [1]. It is recommended to perform the analysis in the MATLAB Simulink environment.

1.1. Need of Hybrid PV and Wind Integration for EV Charging

The integration of hybrid photovoltaic (PV) and wind energy for electric vehicle charging represents a move towards sustainable energy use and is

particularly important in the context of the explosion of the electric vehicle (EV) market. This approach reduces dependence on fossil fuels in line with the environmental goals of electric vehicles by reducing emissions and pollution [2]. This combination increases energy security and independence from production, provides similar energy sources from solar and wind, and provides capital Nature charges electricity everywhere. From a business perspective, the combination of lower costs and the ability to integrate elements such as inverters and battery storage makes the system more profitable over time [3-5]. It is scalable and flexible, can support everything from single chargers to large charging stations and provides grid support during times of

peak demand. Additionally, using renewable energy solutions can help comply with environmental regulations and potentially unlock financial support. For companies, this demonstrates their commitment to sustainability and improving their reputation in the consumer environment [6]. Overall, this collaboration not only addresses sustainable transportation and energy issues but also plays an important role in the global shift towards clean energy and transportation solutions.

1.2. Scope of Research Work

1. **Design and optimization:** Focus on creating efficient and reliable designs for the integration of photovoltaic and wind energy into the grid regarding the connection between us - developing algorithms to increase high-end power and performance [7].
2. **Energy Management and Storage Conservation:** Designed to create an energy management system that balances energy consumption from renewable sources, grids

2. Methodology

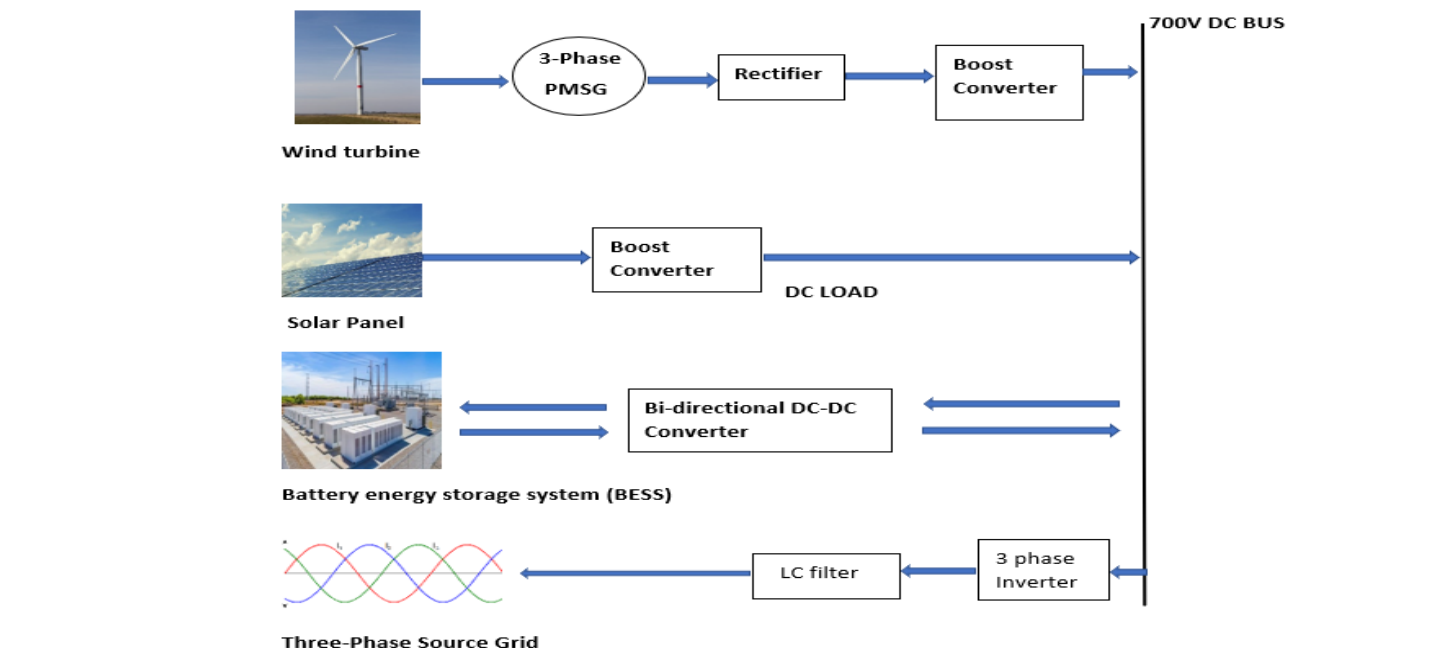


Figure 1 Circuit Topology of the Proposed System

- and storage and optimizes energy storage to keep the electric car paying off [8].
3. **Grid integration and impact analysis:** Identifying and mitigating the impact of grid integration on grid security, including the investigation of technology and control strategies for power and frequency control.

1.3. Objective of Research Work

1. Analyze the energy balance under different irradiance and wind speed conditions [9].
2. Evaluate energy management algorithms for renewable energy and battery storage. Control performance to ensure stable power for continuous charging.
3. Analyze the impact of grid security and make mitigation strategies available.
4. Consider determining costs and revenues and conduct a cost-effectiveness analysis of the business. It emphasizes its contribution to sustainable development by reducing dependence on fossil fuels and reducing emissions [10].

MODE 1: Solar PV with boost converter (250W) and wind panel with rectifier (5.8kW)

In mode 1, the solar power is connected to the boost converter to increase the voltage and the wind panel drag is connected to the rectifier. Income. It is converted from AC to DC. This power is sent to the 700V DC bus and from there it charges the charging stations and BESS. This mode is used when there is sunlight during the day [11].

MODE 2: Windmill with rectifier

Mode 2 has no solar energy at night. In this case, the air panel is connected to the 700V DC bus bar and rectifier. In this mode, we can draw power from BESS to charge the electric car [12].

MODE 3: BESS with Bi-directional DC-DC converter

In mode 3, in some conditions when solar and windmill power is not present, we can take power from BESS with the help of a Bi-directional DC-DC Converter to charge EVs [13].

MODE 4: Grid-connected Inverter

In mode 4, Based on grid voltage we generate the sin-cos reference generation. Inverter controlled by DQ current control concept. The inverter connects to the LC filter and gives to the EV charging Grid [14].

3. Configuration of Hybrid System Proposal

3.1. Solar Panel

Photovoltaic generators are used to power the batteries. A power converter is used to control the flow of energy to the PV array so that it operates at optimal efficiency [15]. The solar panel equation is shown in the Figure 1.

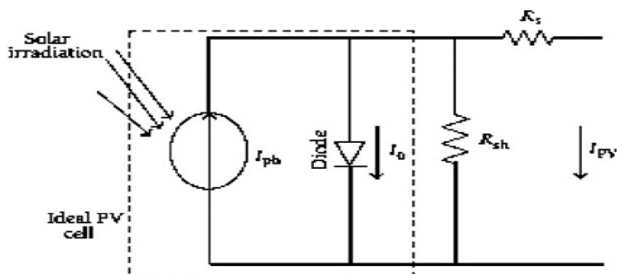


Figure 1 Solar Cell Equivalent Circuit

$$I_{pv} = I_{ph} - I_0 \left\{ \exp \frac{q}{AKT(V_{pv} + I_{pv}R_s)} - 1 \right\} - \frac{V_{pv} + I_{pv}R_s}{R_{sh}} \quad \dots (1)$$

Here I_{pv} is the output current of the photovoltaic cell (A), I_{ph} is the photocurrent, I_d is the diode current, I_{sh} is the current passing through the shunt resistor, I_0 is the reverse saturation current, K , Boltzmann constant = $1.38 \times 10^{-23} \left(\frac{J}{K} \right)$, q , electricity value = 1.6×10^{-19} (G), T is the battery temperature (K), V_{pv} is the photovoltaic cell output voltage (V), A is the best (for crystalline silicon, between 1.2 and 1.6), R_s is the resistance (Ω) and R_{sh} is the balance (Ω). Connect to the switch to get the PV voltage.

$$V_{pv} = -0.411383I_{pv} + \frac{1}{0.86949} \ln \left(1 + \frac{4.682355 * \phi - I_{pv}}{2.35E - 8} \right) \quad \dots (2)$$

The output power from the solar PV array is given by

$$P_{pv} = V_{pv}I_{pv}\eta_{conv} \quad \dots (3)$$

where η_{conv} is DC-DC converter efficiency (typically 90–95%). The simulation diagram of the PV array at different isolation levels is obtained by SIMULINK software. The voltage-current and voltage-output power characteristics of the PV array are shown in Fig 2 and 3 respectively.

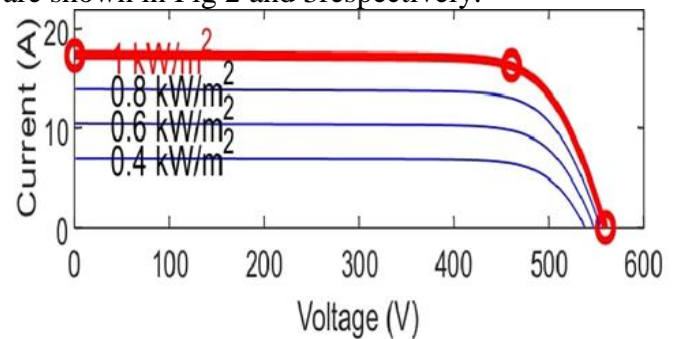


Figure 2 Relation Between Voltage and Current of the PV Array with Varying Irradiation

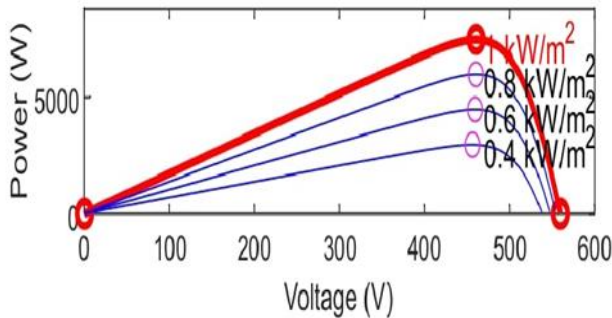


Figure 3 Relation Between Voltage and Output Power of the PV Array with Varying Irradiation

3.2. Incremental Conductance Algorithm

To obtain maximum power from solar PV panels, an MPPT-operated charge controller is introduced in this article (Figure 4). The two main groups of MPPT methods are indirect methods and direct methods. Indirect methods include the constant voltage method, open circuit voltage method, and short circuit current method. In this pursuit, simple assumptions and periodic predictions of MPPT can be made from

simple measurements. For example, the constant voltage generator adjusts the operation of solar photovoltaic modules only in different seasons; For example, the MPP voltage is higher in winter and lower in summer at the same radiation level. This method is not accurate because radiation and temperature change in the same season. Another common indirect MPPT technique is the open circuit voltage (OV) method. In this method, it is assumed that: Where k is a constant and for crystalline silicon its value is usually around 0.7 to 0.8. This method is simple and easy to use compared to other methods. However, the constant k is only approximate, resulting in decreased performance and the system must find a new voltage V_{out} every time lighting conditions change. The load connected to the PV module must be disconnected every time to find a new open source of electricity, resulting in energy loss. The direct MPPT method measures current, voltage or power and is therefore more accurate and sensitive than indirect methods.

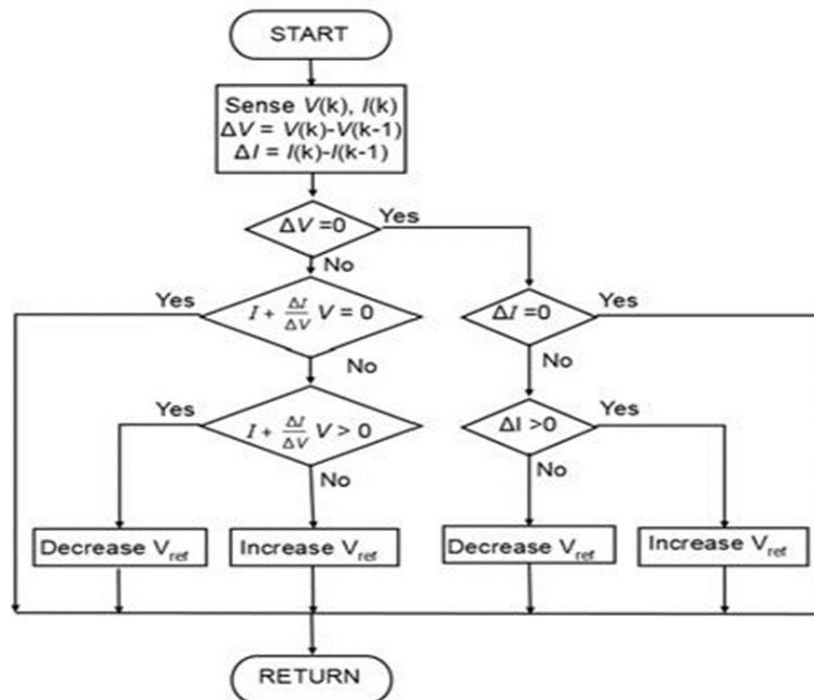


Figure 4 Conductance Algorithm

3.3. Wind Panel

Wind turbines obtain energy from the kinetic energy of the wind. Permanent magnet synchronous generators (PMSG) are used to convert the kinetic energy of wind into electricity. The amount of air coming out of the turbine is proportional to the cube of the air swept by the blades.

$$P_W = \frac{1}{2} C_p(\beta, \lambda) \rho A V^3 \quad \dots (4)$$

Where ρ is the density of air, (kg/m³),
 A is the area swept by blades,
 v is wind speed,
 C_p is the power coefficient of the wind turbine, β is the blade pitch angle, and
 λ is the tip speed ratio.

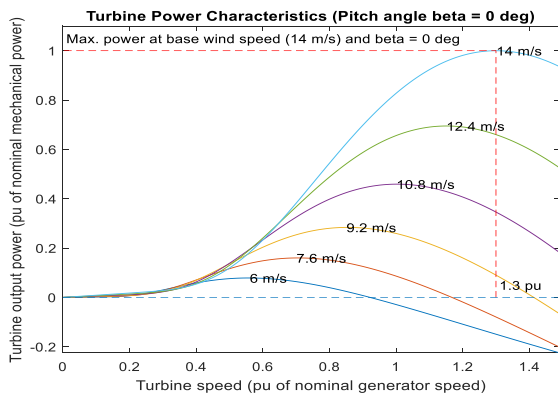


Figure 5 Characteristic Curves of the Wind Turbine When the Power in Per Unit(Pu)

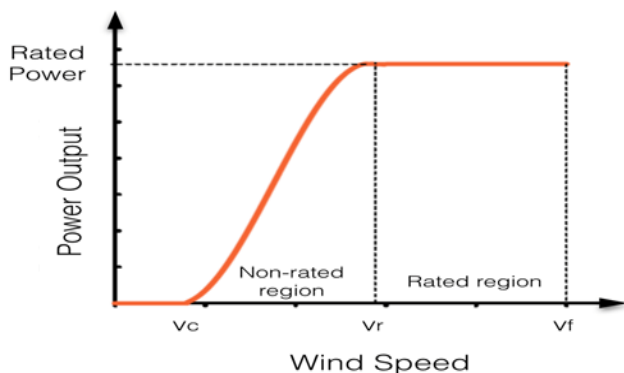


Figure 6 Wind Turbine Characteristics

3.4. Perturb and Observe MPPT Algorithm (P&O)

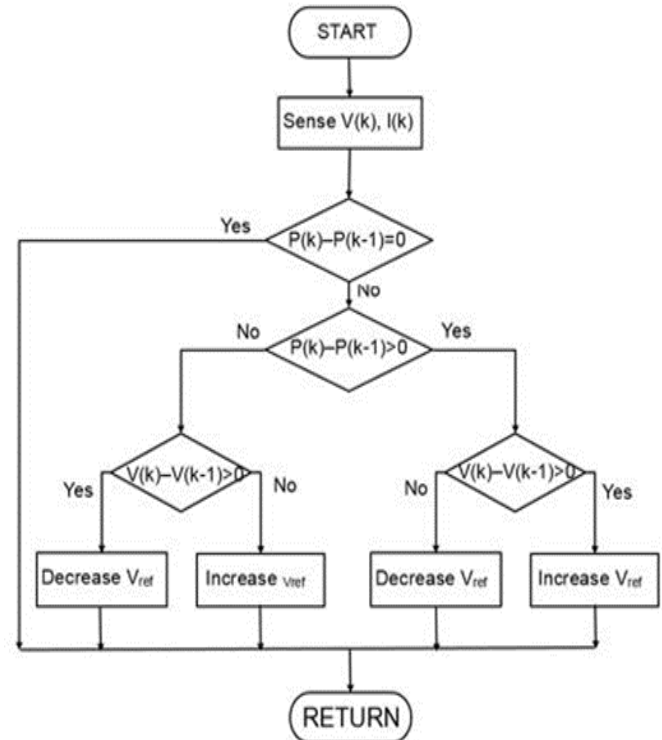


Figure 7 Algorithm of PO MPPT

The P&O method is used to monitor MPP. In this device, small fluctuations occur, which cause the energy to change in the photovoltaic modules. PV output power is usually measured over time and compared to previous power. The same process continues if the output voltage increases, otherwise the effect is reversed. In this algorithm, a perturbation is given to the photovoltaic module or array voltage. Increase or decrease the voltage of the photoelectric module and check whether the power increases. When the increase in voltage causes more power, this means that the operating point of the PV module is to the left of the MPP. Therefore, to achieve MPP, the law needs to have more impact. Conversely, if the increase in voltage leads to a decrease in power, this means that the operating point of the PV module is to the right of the MPP and therefore requires an additional left-hand effect to reach the MPP. The flowchart of the P&O algorithm used by the price

controller is shown in Figures 5 - 7. When the MPPT charge controller connects the PV module to the battery, it measures the PV and battery voltages. Determine whether the battery is fully charged after measuring the battery voltage. If the battery is fully charged, it will stop charging the battery to prevent overcharging. If the battery is not fully charged, charging starts by activating the DC/DC converter. The microcontroller then calculates the current P_{new} power at the output by measuring the voltage and current and compares the calculated power to the previously measured P_{old} power. If P_{new} is greater than P_{old} increases PWM duty to get maximum power from the PV panel. If P_{new} is less than P_{old} , the duty cycle is reduced to allow the

system to return to its previous maximum power. The MPPT algorithm is simple, easy to use, low cost and high accuracy.

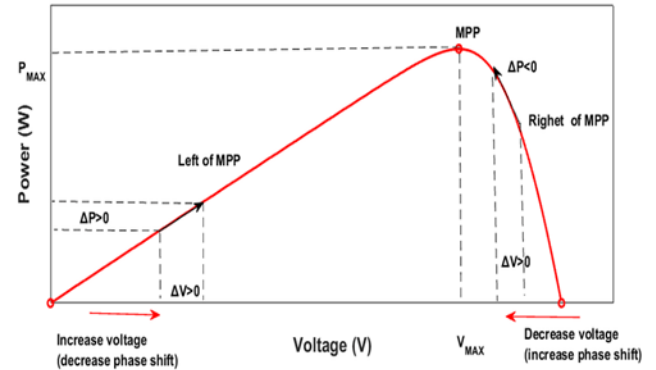


Figure 8 Graph of MPPT algorithm

3.5. Analysis of PMSG

The measurement model of the PMSG takes into account assumptions that are often taken into account in the AC motor model. The electrical balance of the PMSG is used in the (d, q) models to the rotor flux vector are

$$\begin{bmatrix} V_d \\ V_q \end{bmatrix} = \begin{bmatrix} r_s & 0 \\ 0 & r_s \end{bmatrix} \begin{bmatrix} i_d \\ i_q \end{bmatrix} + \frac{d}{dt} \begin{bmatrix} \varphi_d \\ \varphi_q \end{bmatrix} + \omega_r \begin{bmatrix} 0 & -1 \\ 1 & 0 \end{bmatrix} \begin{bmatrix} \varphi_d \\ \varphi_q \end{bmatrix} \dots (5)$$

For distributed sinusoidal back EMF the magnetic flux and current phasors are connected in the following expressions:

$$\begin{aligned} \varphi_d &= L_d i_d + \varphi_r \\ \varphi_q &= L_q i_q \end{aligned} \dots (6)$$

By substituting equations, the following set of equations are obtained by Laplace transform:

$$\begin{aligned} V_d &= (r_s + L_d p) i_d - e_d \\ V_q &= (r_s + L_q p) i_q - e_q \end{aligned} \dots (7)$$

the direct and the quadrature back E.M.F components are expressed as:

$$e_d = \varphi_r L_q i_q$$

$$e_q = \varphi_r L_d i_d + \omega_r \varphi_r \dots (8)$$

The stator's active and reactive powers are given:

$$\begin{aligned} P_s &= \frac{3}{2} (V_d i_d + V_q i_q) \\ Q_s &= \frac{3}{2} (V_q i_d - V_d i_q) \end{aligned} \dots (9)$$

The mechanical equation is expressed as follows:

$$T_m - T_{em} = J \frac{d\theta}{dt} + K_f \theta \dots (10)$$

The electromagnetic torque can be expressed, in the reference frame (d, q), as follows:

$$T_{em} = \frac{3}{2} n_p (\varphi_r - (L_q - L_d) i_d) i_q \dots (11)$$

The control of the stator side converter (SSC) depends on the MPPT tracking maximum power point and prevents the creation of the speed that powers the turbine. The MPPT algorithm provides information about the power used for the engine, so that at any wind speed below maximum, the power is maximum, provides instructions on the use of torque

$$T_m = \frac{1}{2} \rho \pi R_t^3 C_{pmax} V^2 / \gamma_{opt} \dots (12)$$

Where: R_t : Blade radius (m), γ_{opt} : Optimal relative wind speed.

3.6. Boost Converter

To replicate load current modulation, a variable source Boost converter is employed. The Boost converter's schematic diagram analysis using Simulink/MATLAB. The P and O MPPT for variable wind speed of wind turbines and the incremental conductance algorithm for PV panel boost conversion in insolation ranging from 1000 W/m² to 400 W/m² demonstrate the dynamic performance of the boost converter in:

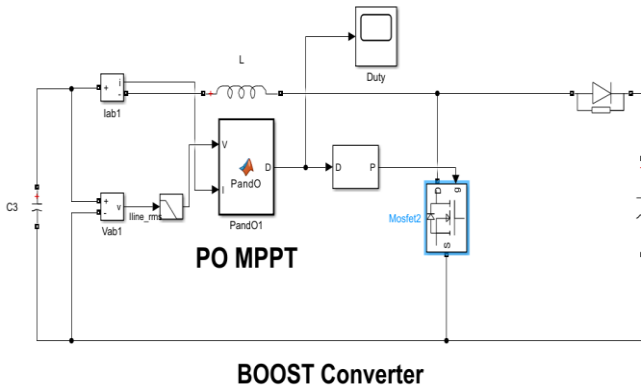


Figure 9 Simulation Blocks Diagram of a Boost Converter with A Wind Turbine

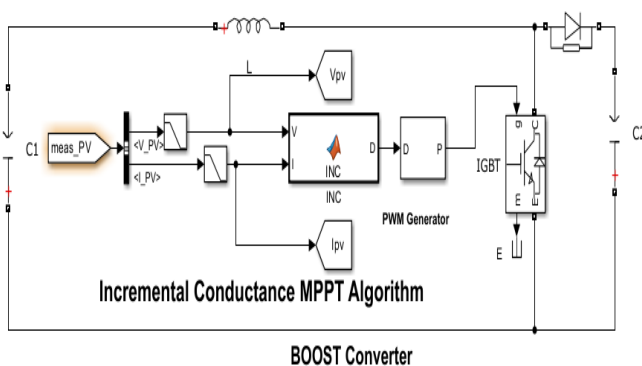
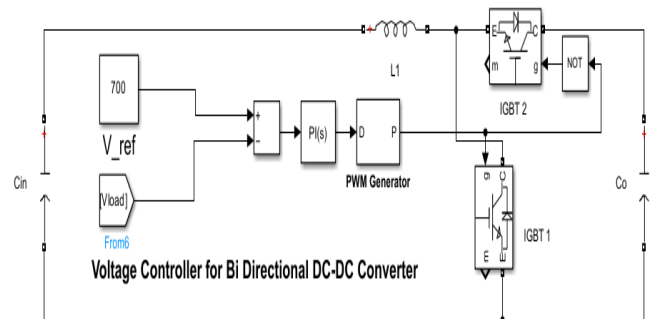


Figure 10 Simulation Blocks Diagram of a Boost Converter with A PV Panel

3.7. BI Directional Dc-Dc Converter

Bidirectional DC-DC converters regulate the DC bus voltage's power flow in both directions. The output

of solar power systems and windmills varies due to variations in the surrounding environment. These energy sources' significant output swings make them unreliable for feeding electricity as a standalone system.



The bidirectional DC/DC converter

Figure 11 Simulation Blocks Diagram of a Bi-Directional Dc-Dc Converter with A Battery Energy Storage System

To regulate the bus voltage, a PI controller is employed. 700V is the reference voltage, and it is contrasted with the immediate bus voltage value for PI controller input error signal calculation. The reference converter current for a current controller in boost or buck mode is the output. The reference converter current establishes the converter's working mode and reflects the direction of the current. Current controllers use the voltage controller algorithm. For engineering applications requiring a basic control framework, the voltage controller algorithm exhibits greater resilience and dependability against external disruptions. It is not required to compute error signal values exactly. In this sense, changes in load disturbance and performance metrics are insensitive to system stability.

3.8. Battery Modelling

The energy stored in the battery is called battery capacity. It is measured in ampere-hours (Ah), watt-hours (Wh), or kilowatt-hours (kWh).

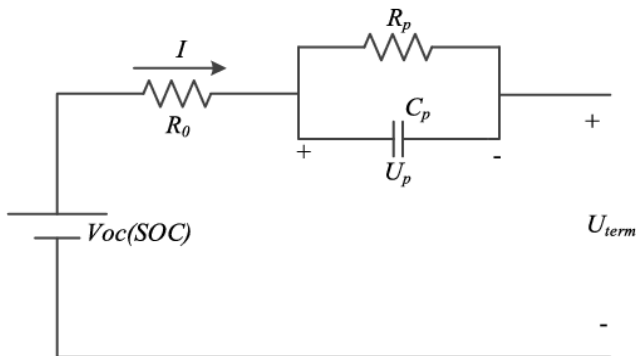


Figure 12 Equivalent Diagram of Battery Circuit Model

A 12V, 48Ah Lithium-ion battery is a type of rechargeable battery. The battery's nominal voltage, which is normally about 12 volts when completely charged, is indicated by the 12V designation. The load conditions and battery state of charge can affect the actual voltage. The battery's capacity is indicated by the 48Ah (Ampere-hour) rating, which shows how much charge the battery can provide over a given amount of time. We have assembled a battery pack system using 35 individual batteries, each rated at 12V. When connected in series, these batteries provide a combined voltage of 420V (12V x 35). The capacity of the entire battery pack is 48Ah, which remains consistent with the capacity of the individual batteries.

3.9. Phase-Locked Loop Algorithm

Phase Locked Loops (PLL) are used in grid-connected power converter topologies to synchronize with the grid voltage. PLL is required to provide sufficient power from the power converter to the grid. PLLs used in renewable energy power converters are reported in studies. PLL can also be used for control and monitoring purposes. PLL is used with a closed-loop control algorithm in a digital controller. Depending on the particular, the digital controller used may be a microcontroller such as a high-end floating-point digital signal processor (DSP), field-programmable gate array (FPGA), or digital signal peripheral interface controller (dsPIC). Depending upon the cost of use and need for difficulty. Synchronous reference phase-locked loop

(SRF-PLL) is a three-phase PLL commonly used in grid-connected power converters. SRF-PLL is used to estimate the frequency and phase of the grid. It extracts unit amplitude sine and cosine signals from the PLL using phase estimation. These are called unit vectors. These vector units are used to generate signals in closed-loop control of the grid-connected power converter. The performance of PLL is affected by the presence of inconsistencies, harmonics and DC drifts in the input voltage. When the input has a DC offset, the estimated frequency and phase have a sinusoidal fluctuation at that frequency. The unit vector produced by the PLL has a DC offset in addition to the ripples. When the input has a DC offset, the result of the DC offset in the unit vector is mathematically proven. For the input DC offset of SRF-PLL, the DC offset in the unit vector can be measured. Traditionally inverter current controllers have a low pass configuration. Therefore, for a conventional current controller design, the gain of the DC closed-loop switch is 1. Therefore, when the house vector used as a reference has a DC offset, DC will be injected into the grid, which is undesirable. This is illustrated by using a grid-tied inverter with electrical distribution equipment such as photovoltaic panels, as shown in Figure 8. Closed-loop control of this inverter generally involves injecting a sinusoidal current into the grid by combining the power. The reference current dq is given in the rotated reference frame. The power consumption consists of $V_{d,ref}$ and $V_{q,ref}$ using vectors as shown in Figure 9. The DC drift at the PLL input is caused by the mismatch between the DC drift in the voltage sensor, the analog-to-digital converter (ADC) and the semiconductor switches in the connected network. However, the advantage of SRF-PLL over higher-order PLL is ease of use. If based on the use of low-level controllers, SRF-PLL will save a lot of digital resources and reduce the computation time. Therefore, when the input has a DC offset, it is necessary to make a detailed design of the simple SRF-PLL. SRF-PLL's design goals

may indicate: For a given worst-case DC offset input, SRF-PLL must produce vectors that meet coupling standards (such as IEEE 1547-2003). For a given worst-case DC offset input, SRF-PLL should be small. This model is useful for the following computations:

- For a known amount of input DC offset, the resulting DC offsets in the unit vectors can be computed.
- Variation of unit vector dc offset versus SRF-PLL bandwidth can be obtained for a given amount of dc offset in the input.
- The effect of unbalance and harmonics can be quantified.

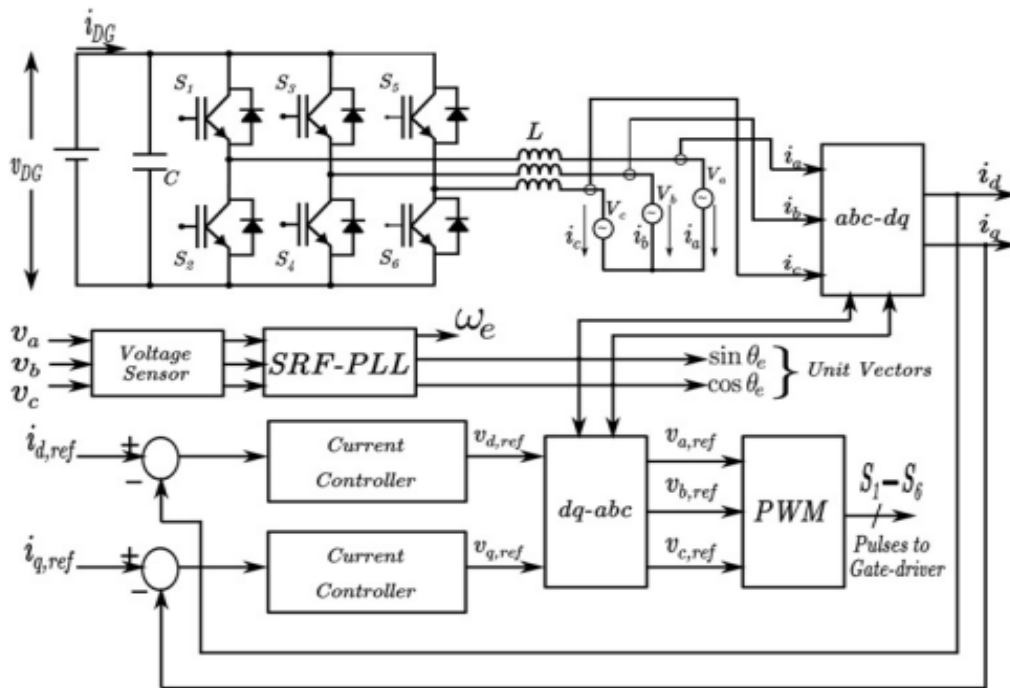


Figure 13 Three-Phase Grid-Connected Inverter and its Closed-Loop Control Implementation Including SRF-PL

3.10. Linear Small-Signal State-Space Modelling of SRF-PLL

As illustrated in Fig 10-13, the SRF-PLL structure. The three-phase detected voltage signals, V_a , V_b and V_c , constitute the input to the PLL. These are two-phase stationary reference frame signals V_α that have been transformed V_β . The stationary frame transformation ($abc - \alpha\beta$) from three phases to two phases is provided by

$$\begin{bmatrix} V_\alpha \\ V_\beta \end{bmatrix} = \begin{bmatrix} \frac{2}{3} & -\frac{1}{3} & -\frac{1}{3} \\ 0 & \frac{1}{\sqrt{3}} & \frac{1}{\sqrt{3}} \end{bmatrix} \begin{bmatrix} V_a \\ V_b \\ V_c \end{bmatrix} \quad \dots (1)$$

It does not employ pre-filters for the basic SRF-PLL. Because of this, the "switch" S in Fig. 14 is maintained in a fashion that allows V_α and V_β to be sent straight into the $\alpha\beta$ to dq rotating reference frame transformation block, which is the next block. This conversion is provided by

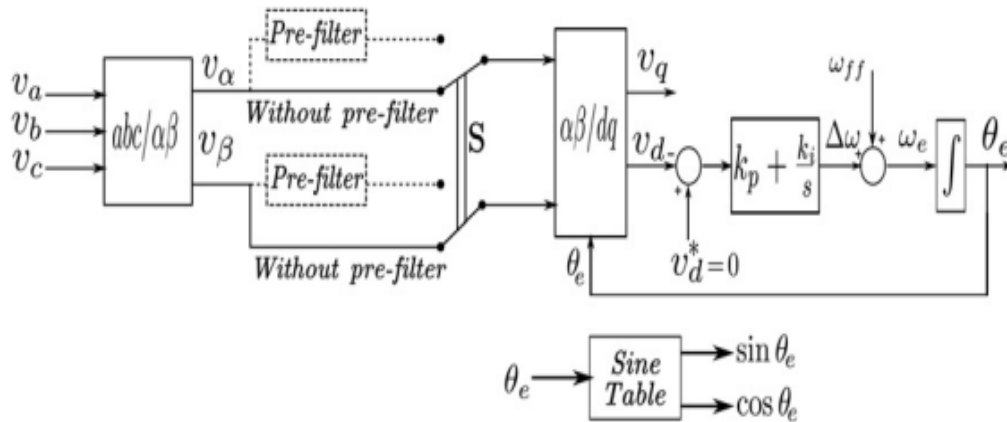


Figure 14 Structure of A Three-Phase SRF-PLL

The Position of the Switch S Determines Whether A DC Blocking Pre-Filter is Included for V_α and V_β . When the grid voltage vector is perfectly aligned along the q-axis, the proportional-integral (PI) controller employed in the PLL guarantees that $V_d = 0$ in the steady state. The PLL yields ω_e, θ_e along with the unit vectors $\sin\theta_e, \cos\theta_e$. The estimated frequency and phase angle are represented by the variables ω_e and θ_e , respectively. These could be thought of as this system's state variable. The shift from a stationary to a rotating reference frame makes this system non-linear.

$$\begin{bmatrix} V_d \\ V_q \end{bmatrix} = \begin{bmatrix} \cos \theta_e & \sin \theta_e \\ -\sin \theta_e & \cos \theta_e \end{bmatrix} \begin{bmatrix} V_\alpha \\ V_\beta \end{bmatrix} \quad \dots (2)$$

These can be taken as the state variables in this system. This system is non-linear due to the stationary to rotating reference frame transformation. From (2), the expression for V_d is

$$V_d = V_\alpha \cos \theta_e + V_\beta \sin \theta_e \quad \dots (3)$$

the derivative of V_d can be computed using (3)

$$\begin{aligned} \dot{V}_d &= V_\alpha \cos \theta_c + V_\beta \sin \theta_c - V_\alpha \omega_c \sin \theta_c \\ &\quad + V_\beta \omega_c \cos \theta_c \quad \dots (4) \end{aligned}$$

In arriving at (4), the following equation is used

$$\dot{\theta}_e = \omega_e \quad \dots (5)$$

The estimated frequency ω_e is given by $\omega_e = -k_p v_d - k_i \int v_d dt + \omega_{ff} \dots (6)$

Thus

$$\omega_e = -K_p V_d - K_i V_d \quad \dots (7)$$

By substitution we get

$$\begin{aligned} \omega_e &= (-K_p v_d - K_p \omega_c V_\beta - K_i V_\alpha) \cos \theta_e + \\ &\quad (-K_p V_\beta + K_p \omega_e V_\alpha - K_i V_\alpha) \sin \theta_e \quad \dots (8) \end{aligned}$$

Where,

$$\begin{aligned} P_1 &= -K_p V_\alpha - K_p \omega_c V_\beta - K_i V_\alpha \\ P_2 &= -k_p v_\beta + k_p \omega_c v_\alpha - k_i v_\beta \quad \dots (9) \end{aligned}$$

The inputs and the state variables are defined as follows

$$\begin{aligned} V_\alpha &= V_{\alpha 0} + V_a; \quad V_\beta = V_{\beta 0} + V_b \\ \omega_c &= \omega_0 + \omega_c \quad ; \quad \theta_c = \theta_0 + \theta_c \quad \dots (10) \end{aligned}$$

Steady-state and steady-state operation of SRF-PLL by design. The purpose of this is to show that the fluctuation in the predicted frequency is negligible in the generated data. The input voltage v_a , in-phase unit vector and predicted frequency for the higher design bandwidth of 200 Hz are shown in Fig 15. Fluctuations in the estimated frequency may occur. At the same time, the waveform formed when the bandwidth is 20.4Hz is shown in Figure 16. It can be

seen that the fluctuation in the estimated frequency is negligible. A phase shift of 60° was applied to each design to examine the steady-state response of SRF-PLL at a design bandwidth of 20.4.

3.11. Three-Phase PWM Bridge Inverter Using MOSFET

Often referred to as inverters, DC to AC converters are split into voltage source inverters (VSI) and current source inverters (CSI) based on the kind of power source and matching power circuit layout. Three-phase VSI with low power consumption is suitable for medium to high-power applications. These topologies are primarily intended to supply a three-phase voltage with controllable amplitude, phase, and frequency. Three-phase DC/AC voltage source inverters are commonly used in motor drives; they actively filter and integrate power flow control in generators and uninterruptible power supplies, producing controllable frequency and AC voltage amplitude. The standard three-phase inverter shown in Figure 17 to 23 has six switches the switching of which depends on the modulation scheme.

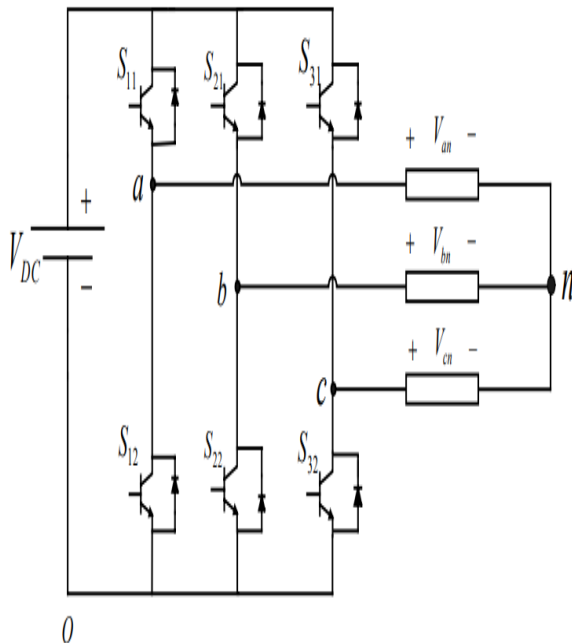


Figure 15 PWM Inverter

The table (1) below lists the eight switch states for the inverter.

Table 1 Inverter has Eight Switch States

S ₁₁	S ₁₂	S ₃₁	V _{ab}	V _{bc}	V _{ca}
0	0	0	0	0	0
0	0	1	0	-V _{DC}	V _{DC}
0	1	0	-V _{DC}	V _{DC}	0
0	1	1	-V _{DC}	0	-V _{DC}
1	0	0	V _{DC}	0	-V _{DC}
1	0	1	V _{DC}	-V _{DC}	0
1	1	0	0	V _{DC}	-V _{DC}
1	1	1	0	0	0

As mentioned before, for the circuit to satisfy KVL and KCL, two switches in the same direction cannot be opened simultaneously because this will cause a short circuit on the electrical input, which violates KVL. Therefore the products of the two keys are equally complimentary

$$S_{11} + S_{12} = 1 \tag{1.1}$$

$$S_{21} + S_{22} = 1 \tag{1.2}$$

$$S_{31} + S_{32} = 1 \tag{1.3}$$

There are eight status switches displayed, and two of them have an output of zero AC voltage. In this instance, neither the upper nor lower component is attached to the AC line anymore. Zero AC output voltage is not produced in other instances. An electrical waveform is produced by the inverter's state transitions. As a result, the AC output line produces a variety of voltage values, including V_{DC}, 0V_{DC}, and -V_{DC}. The modulating technique, which guarantees the usage of only valid states, selects the states to generate the desired waveform.

$$\frac{V_{DC}}{2} (S_{11} - S_{12}) = V_{AN} + V_{NO} \tag{1.4}$$

$$\frac{V_{DC}}{2} (S_{21} - S_{22}) = V_{BN} + V_{NO} \tag{1.5}$$

$$\frac{V_{DC}}{2} (S_{31} - S_{32}) = V_{CN} + V_{NO} \tag{1.6}$$

Applying conditions from 1.2 to 1.4 and expressing the Equations from 1.5 to 1.7 in terms of modulation signals yields

$$\frac{V_{DC}}{2}(M_{11}) = V_{AN} + V_{NO} \quad (1.7)$$

$$\frac{V_{DC}}{2}(M_{21}) = V_{BN} + V_{NO} \quad (1.8)$$

$$\frac{V_{DC}}{2}(M_{31}) = V_{CN} + V_{NO} \quad (1.9)$$

Adding the Equations from 1.5 to 1.7 together gives Equation 2.1 as

$$\frac{V_{DC}}{2}(s_{11} + s_{12} + s_{31} - s_{12} - s_{22} - s_{32}) = v_{AN} + v_{ON} + V_{CN} + 3V_{NO}. \quad (2.1)$$

By dealing with balanced voltages

$V_{AN} + V_{BN} + V_{CN} = 0$, equation (2.1) becomes,

$$\frac{V_{DC}}{6}(2s_{11} + 2s_{21} + 2s_{31} - 3) = v_{NO} \quad (2.2)$$

Substituting for VNO in equations 1.5 to 1.7 gives

$$\frac{V_{DC}}{3}(2s_{11} - s_{21} - s_{31}) = V_{AN}$$

$$\frac{V_{DC}}{3}(2s_{21} - s_{21} - s_{31}) = V_{BN}$$

$$\frac{V_{DC}}{3}(2s_{31} - s_{21} - s_{11}) = V_{CN}$$

With an operating level of $\pm/6$, the line's basic waveform is \pm three times the voltage level. The inverter gets its name from the line waveform's six consecutive waveforms, as seen in the picture. The waveform's typical harmonics are $6n \pm 1$, where n is an integer.

4. Simulation and Results

4.1. PV Measurement

The photovoltaic (PV) power output varies proportionally with irradiance levels, with an initial irradiance of 1000W/m² yielding 7.5kW of power. As irradiance decreases to 500W/m², the PV power output decreases to 3.70kW, and at extremely low levels, such as 10W/m², the PV power output approaches zero watts.

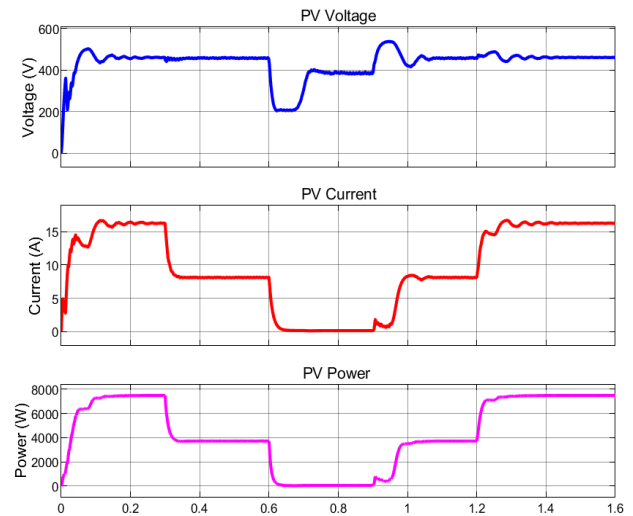


Figure 16 PV Measurement

4.2. Wind Turbine Measurement

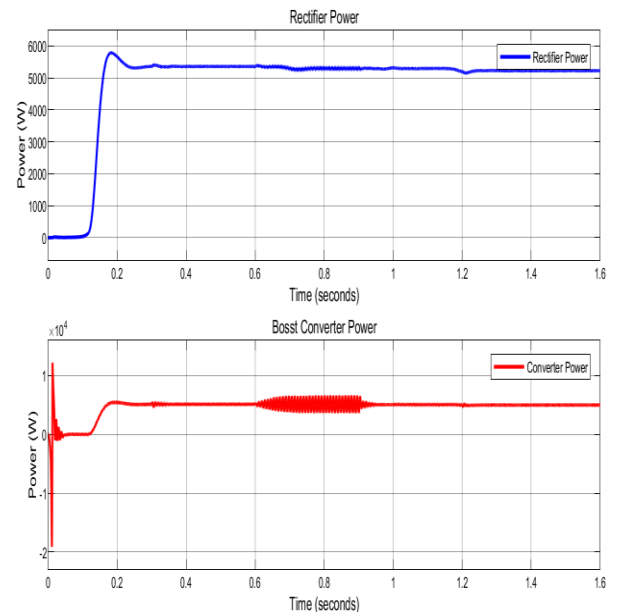


Figure 17 Wind Turbine Measurement

The wind turbine's input parameters include generator speed, pitch angle, and wind speed. Wind speed varies from 12m/s initially to 10m/s after 2 seconds. the output of the wind turbine through the boost converter is 5.5kW.

4.3. DC Load Measurement

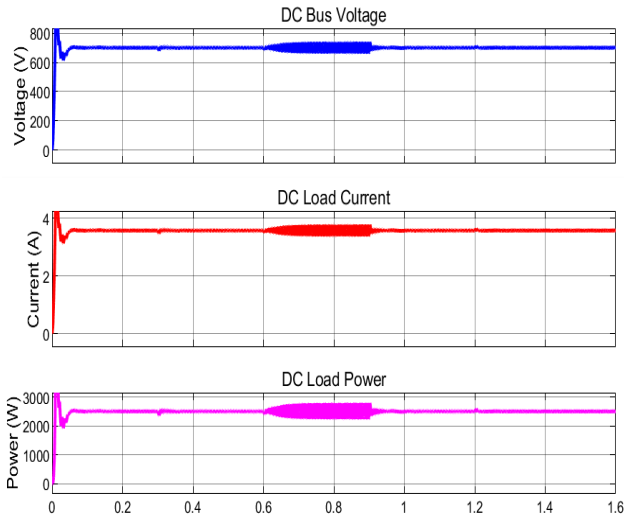


Figure 18 DC Load Measurement

With a maintained DC voltage bus at 700V, the system operates with a DC power output of 2.5kW and a DC bus current averaging around 3.5A.

4.4. Battery Measurement

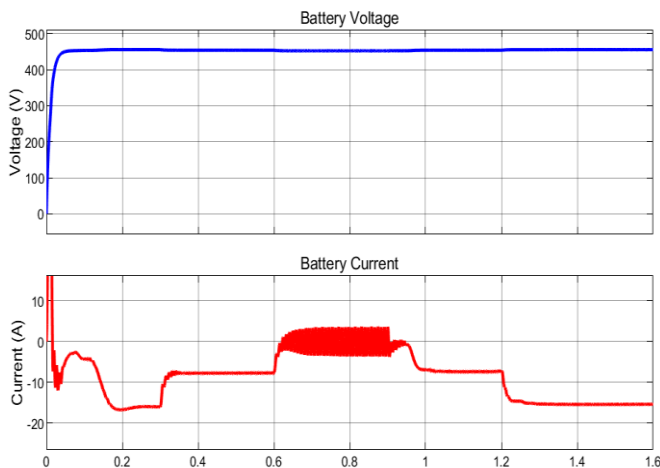


Figure 19 Battery Measurement

At wind speeds of 12m/s, the system generates approximately 5.7kW of power, with the battery operating at a voltage of around 450V. The battery's operation varies dynamically, transitioning to

charging mode when both PV and wind sources produce excess power and switching to discharging mode when PV power diminishes to zero.

4.5. State of Charge

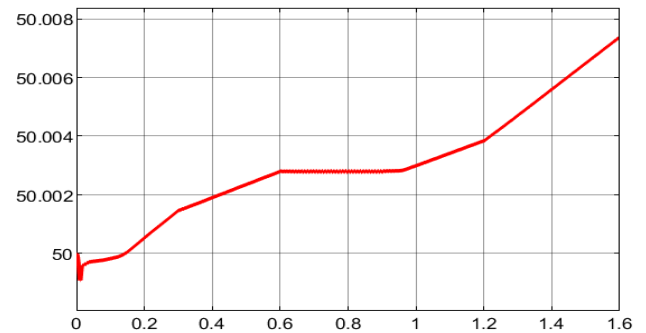


Figure 20 State of Charge

4.6. Grid Measurement

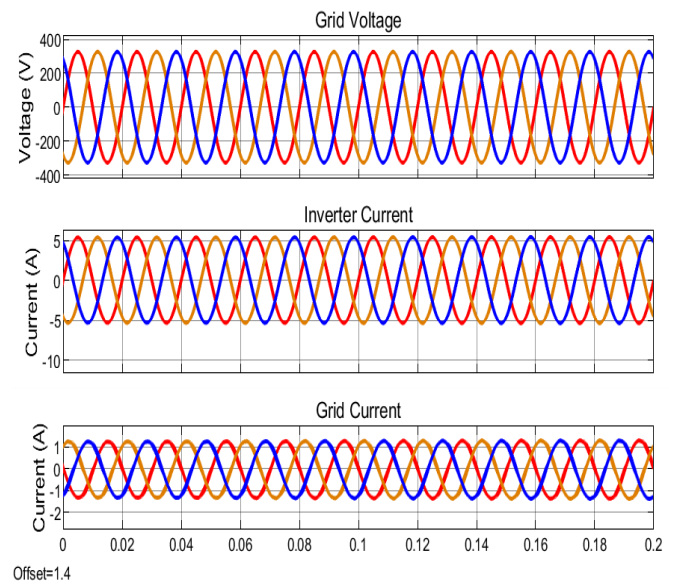


Figure 21 Grid Measurement

The inverter current peak amplitude is regulated at 5A under the condition of PV power greater than 0.5 and state of charge (SOC) above 10%, allowing for power supply to the grid. Conversely, when PV power drops below 0.5 and SOC falls below 10%, the system draws power from the grid.

4.7. AC Load

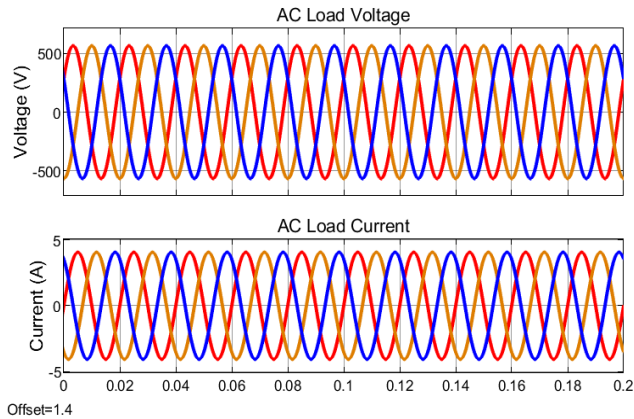


Figure 22 AC Load

4.8. DC Bus Current

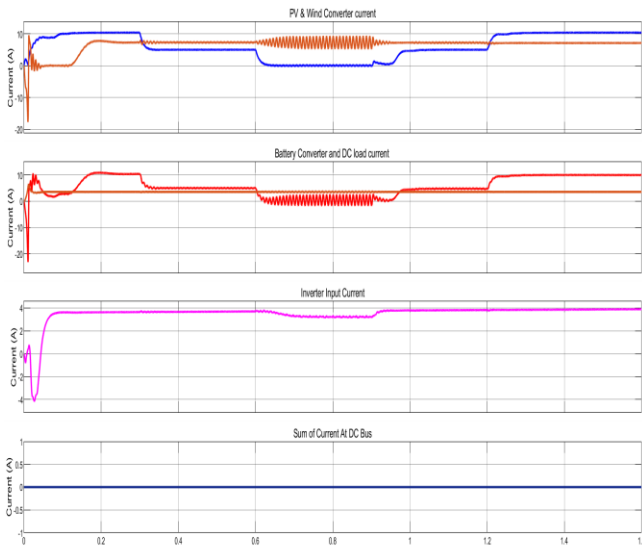


Figure 23 DC Bus Current

The sum of current drawn by the PV and wind converters, battery, DC load, and inverter input is maintained at zero, ensuring power balance between sources and the node. Consequently, the sum of currents at the DC bus remains consistently zero, indicating equilibrium in the system.

Conclusion

The research on a three-phase grid-connected system integrating photovoltaic (PV) panels, wind turbines, and battery storage demonstrates a robust solution for maintaining power balance despite fluctuations in

solar irradiance and wind speed. Through comprehensive modelling and simulation, the system effectively manages and distributes energy, ensuring a stable and reliable power supply to the grid. The dynamic power management capabilities of the system allow it to balance generation from PV and wind sources with battery storage, ensuring that supply matches demand even with variable renewable inputs. Battery storage plays a pivotal role by buffering the intermittency of these sources, storing excess energy during periods of high generation and releasing it during low generation to maintain a continuous power supply. This integration mitigates the impact of rapid changes in renewable output, with advanced control algorithms and power electronics ensuring real-time adjustments for seamless grid integration. The combined use of PV, wind, and batteries not only enhances grid stability and reliability but also provides environmental and economic benefits by reducing dependence on fossil fuels and promoting sustainability. Additionally, the modular nature of the system allows for scalability and flexibility, making it suitable for a wide range of applications from residential to industrial. Overall, the research confirms that a well-coordinated PV-wind-battery system is a viable solution for modern power grids, effectively maintaining power balance and supporting the reliable integration of renewable energy sources.

References

- [1]. "Hybrid solar-wind-powered charging station for electric vehicles", Nilesh Dhongade*1, Rakesh Dhopare*2, Department Of Electrical Engineering, Amrutvahini College Of Engineering, Sangamner, Savitribai Phule Pune University, Pune-402207 India. International research journal of modernization in engineering technology and science, Volume:04/Issue:05/May-2022.
- [2]. "Hybrid Solar-Wind Charging Station for Electric Vehicles and Its Simulation", International Journal for Research in Applied

- Science & Engineering Technology (IJRASET), ISSN: 2321-9653; IC Value: 45.98; SJ Impact Factor: 7.538, Volume 10 Issue VIII Aug 2022.
- [3]. "Solar Based Bi-Directional V2h Charging System", Priyanka K, Bindhu N, Vikas P, K Shanmukha Sundar, Department of Electrical and Electronics Engineering, Dayananda Sagar Academy of Technology and Management, Bangalore, Karnataka, India © 2023 IJCRT | Volume 11, Issue 5 May 2023|ISSN:2320-2882.
- [4]. T. S. Biya and M. R. Sindhu, 2019, "Design and Power Management of Solar Powered Electric Vehicle Charging Station with Energy Storage System", 2019, 3rd Int. conf. on Electronics, Communication and Aerospace Technology (ICECA), Coimbatore, India, pp. 815-820.
- [5]. "Solar and Wind Energy Based Charging Station for Electric Vehicles" by C. Chellaswamy, V. Nagaraju, R. Muthammal. International Journal of Advanced Research in Electrical, Electronics and Instrumentation Engineering, Vol. 7, Issue 1, January 2018.
- [6]. "A Review on Hybrid Solar PV and Wind Energy System" by Nema Parveen, Varsha Sharma. International Research Journal of Engineering and Technology (IRJET), Volume: 05 Issue: 12 | Dec 2018.
- [7]. C. Chellaswamy, R. Ramesh, "Future renewable energy option for recharging full electric vehicles" Renewable and Sustainable Energy Reviews, Vol.76, pp. 824–838, 2017.
- [8]. Fathabadi H. "Plug-in hybrid electric vehicles (PHEVs): replacing internal combustion engine with clean and renewable energy based auxiliary power sources". IEEE Transactions on Power Electronics, 2018, 33(11): 9611–9618.
- [9]. "Design of synchronous reference frame phase-locked loop with the presence of DC offsets in the input voltage", ISSN 1755-4535, Received on 16th April 2015, Revised on 17th July 2015, Accepted on 23rd August 2015, doi: 10.1049/ietpel.2014.0878www.ietdl.org,
- Abhijit Kulkarni, Vinod John Department of Electrical Engineering, IISc Bangalore, Bengaluru, Karnataka, India.
- [10]. "A Novel Bidirectional DC-DC Converter for Dynamic Performance Enhancement of Hybrid AC/DC Microgrid", Morteza Daviran Keshavarzi and Mohd Hasan Ali, Department of Electrical and Computer Engineering, University of Memphis, Memphis, TN 38152, USA, Received: 16 September 2020; Accepted: 4 October 2020; Published: 11 October 2020.
- [11]. "Grid integration of PMSG-based wind energy conversion with battery storage system" Venkatachalam K M, V. Saravanan, International Journal of Applied Power Engineering (IJAPE) Vol. 10, No. 1, March 2021, pp. 48~57 ISSN: 2252-8792, DOI: 10.11591/jape.v10.i1.pp48-57.
- [12]. "Modelling and Charge-Discharge control of Li-ion Battery using Simulink" March 2023 | IJIRT| Volume 9 Issue 10 | ISSN: 2349-6002.
- [13]. "Bidirectional dc to dc Converters: An Overview of Various Topologies, Switching Schemes and Control Techniques". Deepak Ravi1, Bandi Mallikarjuna Reddy2, Shimi S.L.3, Paulson Samuel 4 Article in International Journal of Engineering and Technology, September 2018.
- [14]. He, G., Xu, D., Chen, M.: 'A novel control strategy of suppressing DC current injection to the grid for single-phase PV inverter', IEEE Tran. Power Electron., 2015, 30, (3), pp. 1266–1274.
- [15]. "Methodology for the Optimal Design of a Hybrid Charging Station of Electric and Fuel Cell Vehicles Supplied by Renewable Energies and an Energy Storage System" by Higinio Sánchez-Sáinz, Carlos-Andrés García-Vázquez, Francisco L Ilorens Iborra and Luis M. Fernández-Ramírez. Published: 17 October 2019 DOI:10.3390/su11205743.